Long-time stability of a low-energy electron diffraction spin polarization analyzer for magnetic imaging

F. Lofink,[1,a)] S. Hankemeier,[1] R. Frömter,[1] J. Kirschner,[2] and H. P. Oepen[1]
[1]*Institut für Angewandte Physik, Universität Hamburg, Jungiusstr. 11, 20355 Hamburg, Germany*
[2]*Max-Planck-Institut für Mikrostrukturphysik, Weinberg 2, 06120 Halle, Germany*

(Received 22 December 2011; accepted 30 January 2012; published online 17 February 2012)

The time stability of a polarization analyzer that is used for imaging of magnetic structures in a scanning electron microscope with spin polarization analysis (spin-SEM or SEMPA) is investigated. The detector is based on the diffraction of low-energy electrons at a W(100) crystal at 104.5 eV (LEED detector). Due to the adsorption of hydrogen from residual gas, a change of the scattering conditions is found that causes an angular shift of the LEED beams as well as changes of intensity. The quality factor, which describes the efficiency of the detector in SEMPA application, however, is found to be almost constant up to a hydrogen coverage of $\theta \approx 0.25$. This gives stable working conditions within roughly 1 h at vacuum conditions of 10^{-10} mbar. © *2012 American Institute of Physics*. [http://dx.doi.org/10.1063/1.3685629]

I. INTRODUCTION

The scanning electron microscope with polarization analysis (spin-SEM or SEMPA) is a unique instrument for mapping the magnetization distribution at ferromagnetic surfaces. The discovery that low-energy secondary electrons (SE) generated at the surface of a ferromagnetic sample exhibit a high spin polarization P that comes in unison with high intensity has triggered the development of SEMPA.[1–4] SEMPA has a high surface sensitivity, which is caused by energy losses due to Stoner excitations[5,6] and ordinary electron-hole scattering in the cascade process at low energies. This loss channel and the large scattering cross section for minority electrons act as a spin filter which causes the high spin polarization of the SE.

Today, SEMPA is a well-established technique for imaging of magnetic structures scaling from a few hundred microns down to nanometers. The SE-polarization vector is measured point by point, which yields a direct map of the magnetization orientation, i.e., the domain pattern. Presently, three different types of detectors are used in SEMPA: (I) In high-energy (20–100 keV) Mott detectors the polarization sensitivity stems from scattering of electrons at atom cores.[7–10] (II) LEDS (low energy diffuse scattering) detectors use the diffuse scattering at amorphous films,[11] and (III) the LEED (low energy electron diffraction) detector utilizes the electron diffraction at a tungsten single-crystal surface.[12] In the LEED detector the intensity asymmetry of complementary (2, 0) LEED beams is used to analyze the spin polarization of the secondary electrons. The LEED detector has an advantage over the other detectors as it comes with an intrinsic energy filter, which automatically discriminates electrons that have been inadvertently created at some electron-optical element. SEs that originate from the sample have the correct energy, are scattered into the correct angle, and are used for spin detection. The spin sensitivity S is similar for Mott and LEED detectors, while the sensitivity of the LEDS detector is significantly lower (0.27 and 0.10, respectively).[13–15] The latter makes the LEDS detector susceptible to instrumental asymmetries and enforces delicate corrections.[16] The best working point for the LEED detector was found for the (2, 0) LEED beams at a scattering energy of 104.5 eV.[17]

To optimize the LEED detector for spin-SEM application, an adaptation of the detector to the prerequisites that are given by the SE emission process has been made recently. The detector has been redesigned to accept electrons with a wider spread of energies. To quantify the detector performance for spin-SEM application, the detector quality $Q = 2{*}A^2{*}T$ has been introduced.[13] $T(E)$ is the total transmission of the electron optics including the detector and A is the achieved image asymmetry. Q is meant to replace the figure of merit, which is commonly used to quantify spin detectors used for spectroscopy purposes.

Due to the high surface sensitivity of LEED, the working condition of the detector and thus its quality Q is sensitive to contamination, which in SEMPA mainly results from adsorption of residual gases like hydrogen and/or carbon oxides. The LEED pattern can be completely altered by just a low coverage of adsorbates, which in turn can drastically reduce the quality of the spin-analyzing process. This puts severe demands on the vacuum conditions in a spin-SEM based on LEED- or LEDS-detectors. However, these prerequisites are not a real drawback, as the SE emission process at the sample already demands for the same or even better quality of the vacuum conditions. Nevertheless, the susceptibility of the detector to contamination is an important parameter to consider in the application for spin-SEM. A decrease of image quality over time is commonly expected due to the degradation of surface quality of the detector crystal, which was actually found in studies performed with detectors optimized for spectroscopic applications.[18,19]

In this paper we present an investigation of the development of scattering intensity and asymmetry with time that

a)Electronic mail: flofink@physik.uni-hamburg.de. Tel.: +49 (40) 42838-3312. Fax: +49 (40) 42838-2028.

can be used to infer on the changes of the detector quality Q. The consequences for the application of the LEED detector in spin-SEM and the utilization of the behavior as diagnostic tool are discussed.

II. EXPERIMENTAL

The experimental setup, as well as a detailed discussion of the energy filtering and transmission properties of the detector system, has been published recently.[13] The LEED detector was optimized with respect to its application for SEMPA. The new realization allows taking overview images in less than a minute and high quality images within 5–10 min using a primary beam current of about 5 nA. In contrast to a classical analyzer used in spectroscopy that is designed for an energy width of about 0.5 eV,[20] a detector optimized for SEMPA needs a broader energy acceptance. The new design can accept SE of nominally 10 eV energy spread. As the polarization decreases with increasing energy of the SEs the net polarization is reduced, which is, however, outweighed by the gain in intensity, when considering the signal-to-noise ratio of a polarization map obtained in a given measurement time.[21,22] The best performance (highest Q) is now achieved at the scattering potential of 102.5 eV.

The experiments were performed in the following sequence: The detector crystal is flash heated to temperatures of about $T \approx 2500$ K for 10 s, which produces a clean W(001) surface.[23,24] Then, the time evolution of the detector properties is measured as function of the delay time after flash cleaning. The base pressure (mainly hydrogen) is 3×10^{-10} mbar.

To estimate the time interval in which thermal effects will affect the scattering conditions we studied the cooling behavior of the tungsten crystal after flash heating, both experimentally and numerically. Below 500 K the temperature evolution was measured experimentally via a thermocouple, which was directly attached to the crystal. The numerical analysis was performed utilizing the COMSOL-Multiphysics code,[25] which is a finite-element-based simulation tool. The results are shown in Fig. 1. The temperature of the tungsten crystal was simulated as 3D heat transfer with analysis of the temporal evolution. The flash heating was modeled as a heating period of 10 s with a power of 150 W, which are the standard operating parameters in our application. The thermal relaxation of the crystal was modelled assuming heat transfer via radiation and heat flow to a thermally coupled reservoir. To describe radiation cooling a hollow steel sphere with radius of 10 mm and thickness of 0.2 mm was placed around the crystal. The crystal dimensions are 10 mm × 7 mm × 0.5 mm. The outside of the sphere and the reservoir was set to a fixed temperature of 300 K, which let the inner surface of the sphere cool down to 300 K within 5 s after the end of the flash. The size of the reservoir was adjusted so that the simulation result corresponds to the measured thermal behavior below 500 K.

An influence of thermal expansion that could lead to a tilting of the crystal or any curvature of the surface can be ruled out, because the time evolution of the intensities of the four (2, 0) diffraction beams is always symmetric in the experiment.

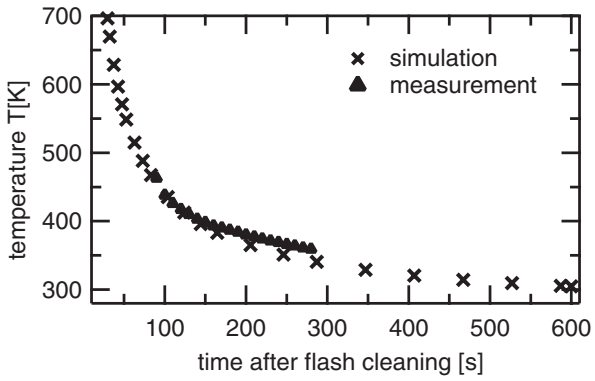

FIG. 1. Temperature evolution of the tungsten crystal during cooling after flash cleaning. The triangles give the results of temperature measurements via thermocouple. The crosses are simulated utilizing COMSOL-Multiphysics. The crystal is heated up to 2500 K during flash cleaning and regains ambient values after 10 min.

III. RESULTS AND DISCUSSION

In a first step, we use SEs that are created at an oxidized copper surface to obtain a SE emission of unpolarized electrons that do not vary with time. By scanning the crystal potential, i.e., the scattering energy, at different times after heating we study the impact of adsorption on the scattering conditions. In Fig. 2, intensity versus potential plots are shown for three different times after flashing. As the detector geometry is fixed to accept electrons that are diffracted into a given scattering angular range, i.e., the (2, 0) beams of W(001) at 104.5 eV, the results of the scans cannot be directly compared to the well known I-V curves.[20] Despite the broad energy window, the diffraction beams are moved across the detector facilities. The result can be roughly understood as a superposition of monochromatic profiles at slightly varying energies convolved with the beam profile. Changes of the scattering potential from the nominal value should cause a

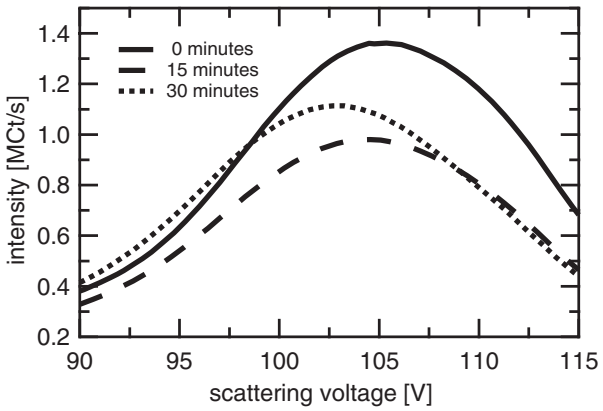

FIG. 2. Intensity distribution as function of the scattering potential at the W(001) crystal for different times after flash cleaning. The asymmetric shape of the curves reflects the asymmetric energy filtering distribution.[13] Analyzing the intensity maximum and its position gives the results shown in Figs. 3(a) and 3(b).

decrease of the intensity. In particular, a change of ±5 V around 102.5 V gives a theoretical intensity decrease of 4%.[13] The variation of the intensity maxima between the three curves is much larger than 4% which obviously comes from a change of the scattering conditions. Thus, from the intensities we can infer on the reflectivity of the diffraction process and this scan can serve as a fingerprint of the surface conditions of the crystal.

Immediately after flash cleaning, the peak of the intensity distribution (1.35×10^6 counts) is located at a potential of 105.4 V. After 15 min the peak has shifted to 104.6 V and the intensity has decreased by ~30% (0.95×10^6 counts). After another 15 min the peak has further moved to 102.7 V, while the intensity has slightly increased to 1.1×10^6 counts. Thus, we observe a time-dependent peak shift as well as a significant variation of intensity.

After flash heating, the crystal passes over a cooling period of 10 min from 2500 K to room temperature, as shown in Fig. 1. Meanwhile, the scattering properties of the crystal are changing, which is caused by the strongly energy-dependent Debye-Waller factor.[26] The maximum transmission is obtained at a scattering potential of 104 V for the clean crystal at room temperature as found earlier.[13] As one can expect, this clean-crystal situation was achieved immediately after cooling down to room temperature, because the sticking probability for $T > 500$ K is negligibly small.[29]

In Fig. 3(a) the evolution of the position of the intensity maximum is plotted versus time. The peak shifts nearly linearly from 105 V to 101 V during the first 60 min. The first data point in Fig. 3(a) does not fit into this trend as it lies within the cooling period after the flash heating. After 60 min a clear kink in the curve is visible and the rate of change becomes smaller. The time evolution of the intensity exhibits a different behavior, which is plotted in Fig. 3(b). For the first 60 min a strong non-monotonic intensity variation is observed which passes over into a slow, linear decrease of intensity after 60 min. For both plots a fast change appears in the first 60 min while beyond that time a slow change is found. In conclusion, the results of Figs. 3(a) and 3(b) reveal that the scattering conditions of the W(001) surface change with time after flash cleaning. Two different time dependencies are found indicating that two different processes are involved.

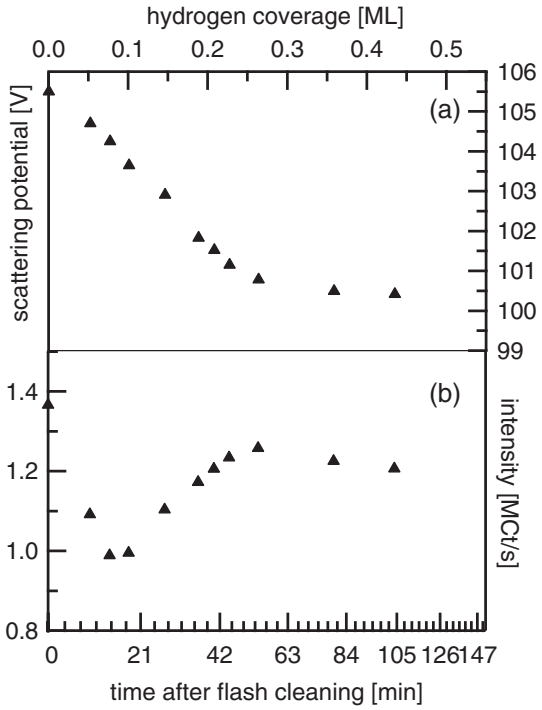

FIG. 3. Evolution of (a) peak position and (b) peak intensity as function of time after flash cleaning. The data have been extracted from intensity curves like the examples given in Fig. 2. Corresponding hydrogen coverages are indicated on the top axis and deduced as described in the text. The nonlinear time axis reflects the coverage dependent sticking probability for the experimentally determined partial pressure for hydrogen.

Possible reasons for a beam shift of a LEED spot as observed in Fig. 3(a) are changes in temperature, interlayer spacing, or the inner potential. Because temperature effects can only be the origin in the first 10 min, a variation of interlayer spacing or inner potential must be the cause of the shift thereafter. From literature it is known that the adsorption of hydrogen on a W(001) surface has a strong influence on both, interlayer spacing and inner potential.[27–31] It was shown that with increasing hydrogen coverage the major peaks in the I-V-curve shift towards lower energies until saturation. This beam shift is in the range of about 3 eV. The dominating effect is believed to come from the variation of interlayer spacing.[28] The studies of King and Thomas[29] show that the interlayer spacing shifts from 1.48 Å for the clean surface to 1.51 Å at hydrogen saturation ($\theta = 1$). This shift is already completed at a coverage of about $\theta \approx 0.25$.[28] Based on these findings one can associate the kink in Fig. 3(a) (60 min) with a hydrogen coverage of $\theta \approx 0.25$. This allows determining the hydrogen pressure when the coverage dependent H_2 sticking probability is accounted for.[28] A hydrogen pressure of 3×10^{-10} mbar has to be assumed in the vicinity of the tungsten single crystal. With this number we can recalibrate the time into hydrogen coverage (upper axis in Fig. 3). The temperature-dependent change of the sticking-probability, which is only significant in the first minute, has been neglected in the calculation.

This gives the following surface and diffraction conditions: In the beginning the W(001) has an ordered (1×1) surface structure. The structure is undergoing several ordered phase transitions during the first 60 min to become an almost ordered hydrogen-induced $\sqrt{2} \times \sqrt{2}$ surface at a coverage of about $\theta \approx 0.25$ (associated with the kink in Fig. 3(a)).[29,30] A phase transition to a disordered surface follows. The disordering process above $\theta \approx 0.25$ causes random scattering and decreases the intensity as well as the asymmetry of the LEED beams.[28] This explains the intensity decrease above $\theta \approx 0.25$ (60 min) in Fig. 3(b). The ordered surface reconstructions up to $\theta \approx 0.25$ (60 min) produce superstructures and domains, which cause intensity variations of the major peaks. However, the exact course of these intensity variations can only be reproduced by full dynamical LEED calculations. This is out of the scope of this work. Above a coverage of about $\theta = 0.4$ the surface slowly turns into a hydrogen–induced, ordered 1×1 surface structure, which is completed at saturation.

The remaining question is how peak shift and intensity variation influence the quality Q of the detector at its working point. To determine the impact on the quality, we

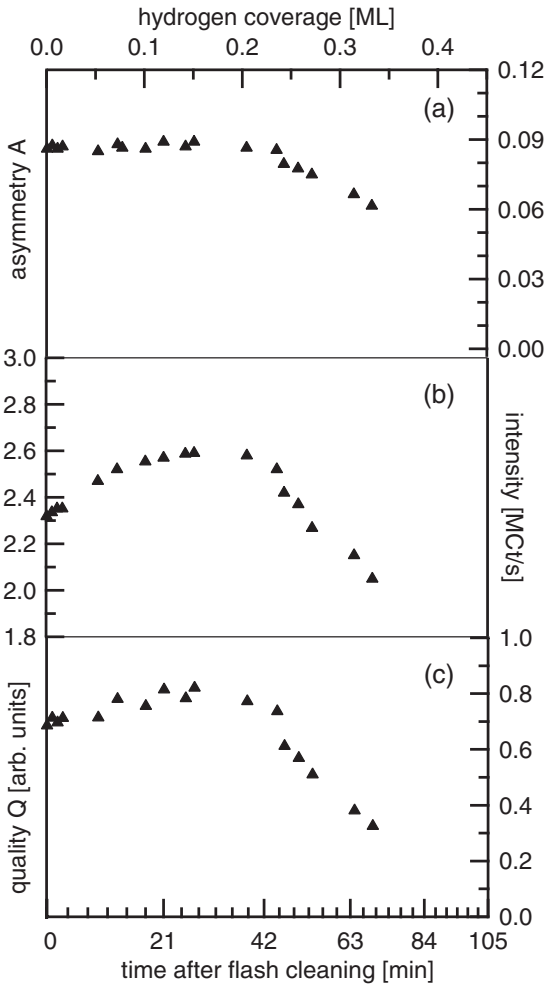

FIG. 4. The variation in the achieved asymmetry of two opposite (2, 0)-beams diffracted from W(001)@102.5 V is shown in (a). (b) The detected intensity. (c) Derived detector quality $Q = 2A^2T$. The measured values are obtained via repeated imaging of the same three-magnetic-domain area of an iron whisker. Corresponding hydrogen coverages are indicated on the top axis and deduced as described in the text. The nonlinear time axis reflects the coverage dependent sticking probability for the experimentally determined partial pressure for hydrogen.

determined the evolution of asymmetry and intensity over time by imaging the magnetic domains of an Fe(100) single crystal (Fe-whisker). The results are presented in Fig. 4. The recording time is 8 min for an image which yields a time resolution of ±4 min for the asymmetry. Figure 4(b) displays the intensity variation which shows a weak increase up to $\theta \approx 0.25$ and a significantly faster decline thereafter. The different shape of the curve compared to Fig. 3(b) is due to the fact, that the scattering potential is kept fixed and the intensity maxima of the (2, 0) LEED beams (Fig. 2) move across the detector window. Within the first 60 min the measured magnetic asymmetry (Fig. 4(a)) is almost constant and centered around a value of 9%. Again, the decrease in asymmetry starts at the point where the peak shift terminates (Fig. 3(a)). This indicates that the asymmetry is not susceptible to the ordered surface reconstructions of the tungsten single crystal. Because of the quadratic dependence of the quality on the asymmetry, this fact is crucial for the long-time stability of the spin detection ability.

The time dependence of the detector quality is shown in Fig. 4(c). Up to a hydrogen coverage of $\theta \approx 0.25$ we obtain a nearly unchanged quality. The optimum working range is between $0.1 < \theta < 0.3$. One might expect that the quality increases again when the surface exhibits an ordered structure at saturation. But this effect is counterbalanced by adsorption of other components of residual gas, such as CO, that cause an increase of random scattering, which leads to a broadening of the LEED beams and therefore a significant decrease of the detected intensity as well as asymmetry.

In conclusion we want to emphasize that the results of this study can be used for the characterization as well as the optimization of a LEED detector for magnetic imaging (SEMPA). On the one hand, the results document that the hydrogen-induced ordered reconstruction of the W(001) single crystal surface has no significant impact on the detector quality. This gives nearly constant imaging conditions until finally the onset of the disordering process at times in the range of one hour sets in (most likely amplified by CO contamination). Consequently, it is necessary to flash clean the crystal after 60 min to keep constant imaging conditions.

On the other hand, the hydrogen pressure around the detector is usually not well known. We present a diagnostic procedure to determine this pressure: By observing the time dependence of the peak shift of the (2, 0)-beam one can easily estimate the amount of hydrogen in the vicinity of the crystal. The information is important to characterize as well as to optimize the LEED detector for SEMPA in order to achieve long time stability of the spin-detection process.

ACKNOWLEDGMENTS

Financial support by Deutsche Forschungsgemeinschaft (DFG) via SFB 668 is gratefully acknowledged. H.P.O. would like to thank CIC nanoGUNE for hospitality during his sabbatical stay and the Basque Foundation for Science for financial support within Ikerbasque fellowship program.

[1]G. Chrobok and M. Hofmann, Phys. Lett. A **57**, 257 (1976).
[2]J. Kirschner and R. Feder, Phys. Rev. Lett. **42**, 1008 (1979).
[3]H. Hopster, R. Raue, E. Kisker, G. Guntherodt, and M. Campagna, Phys. Rev. Lett. **50**, 70 (1983).
[4]E. Kisker, W. Gudat, and K. Schroder, Solid State Commun. **44**, 591 (1982).
[5]J. Kirschner, Phys. Rev. Lett. **55**, 973 (1985).
[6]G. C. Wang, B. I. Dunlap, R. J. Celotta, and P. T. Pierce, Phys. Rev. Lett. **42**, 1349 (1979).
[7]K. Koike and K. Hayakawa, Jpn. J. Appl. Phys. **23**(3), L187 (1984).
[8]R. Allenspach, J. Magn. Magn. Mater. **129**, 160 (1994).
[9]T. Kohashi, M. Konoto, and K. Koike, J. Electron Microsc. **59**(1), 43 (2010).
[10]T. J. Gay and F. B. Dunning, Rev. Sci. Instrum. **63**, 1635 (1992).
[11]J. Unguris, D. T. Pierce, and R. J. Celotta, Rev. Sci. Instrum. **57**, 1314 (1986).
[12]H. P. Oepen and J. Kirschner, Scanning Microsc. **5**, 1 (1991).
[13]R. Frömter, S. Hankemeier, H. P. Oepen, and J. Kirschner, Rev. Sci. Instrum. **82**, 033704 (2011).
[14]T. Kohashi, M. Konoto, and K. Koike, Jpn. J. Appl. Phys. **45**, 6468 (2006).
[15]J. Unguris, *Experimental Methods in the Physical Sciences*, edited by M. De Graef and Y. Zhu (Academic, San Diego, 2001), Vol. 36, p. 167.
[16]M. R. Scheinfein, J. Unguris, M. H. Kelley, D. T. Pierce, and R. J. Celotta, Rev. Sci. Instrum. **61**, 2501 (1990).
[17]J. Kirschner, *Polarized Electrons at Surfaces* (Springer-Verlag, Berlin, 1985).

[18]D. Yu, C. Math, M. Meier, M. Escher, G. Rangelov, and M. Donath, Surf. Sci. **601**, 5803 (2007).
[19]J. Sawler and D. Venus, Rev. Sci. Instrum. **62**, 2409 (1991).
[20]J. Kirschner and R. Feder, Surf. Sci. **103**, 75 (1981).
[21]H. P. Oepen and H. Hopster, *Magnetic Microscopy of Nanostructures*, edited by H. Hopster and H. P. Oepen (Springer, Berlin, 2005), p. 137.
[22]R. Allenspach, IBM J. Res. Dev. **44**, 553 (2000).
[23]R. Cortenraad, S. N. Ermolov, V. N. Semenov, A. W. D. van der Gon, V. G. Glebovsky, S. I. Bozhko, and H. H. Brongersma, J. Cryst. Growth **222**, 154 (2001).
[24]K. Zakeri, T. R. F. Peixoto, Y. Zhang, J. Prokop, and J. Kirschner, Surf. Sci. Lett. **604**, L1 (2010).
[25]See http://www.comsol.com/ for COMSOL, Inc.
[26]J. Kirschner and R. Feder, Surf. Sci. **104**, 488 (1981).
[27]K. Yonehara and L. D. Schmidt, Surf. Sci. **25**, 238 (1971).
[28]K. Christmann, Surf. Sci. Rep. **9**, 1 (1988).
[29]D. A. King and G. Thomas, Surf. Sci. **92**, 201 (1980).
[30]R. A. Baker and P. J. Estrup, J. Chem. Phys. **74**, 1442 (1981).
[31]G. C. Wang, J. Unguris, D. T. Pierce, and R. J. Celotta, Surf. Sci. **114**, L35 (1982).